Microstructural Brain Damage in Patients with SLE: An Analysis using Automated Segmentation of Nerve Tracts from Diffusion MRI

Anna Wikström

Lund, June 2020

Supervisor: Markus Nilsson
Master's Thesis in Biomedical Engineering

LUND UNIVERSITY

LTH
FACULTY OF ENGINEERING

Department of Biomedical Engineering

Abstract

Systemic Lupus Erythematosus, SLE, is a disease with a large variation of symptoms. Some patients have neuropsychiatric symptoms, such as cognitive dysfunction and epilepsy. The classification of patients into NPSLE, with neuropsychiatric symptoms, and non-NPSLE, without these symptoms, is uncertain. Studying the white matter microstructure of SLE patients and comparing this with healthy controls can lead to better understanding of the disease and the neuropsychiatric symptoms. White matter microstructure can be characterized by the use of diffusion MRI. This imaging technique also enables segmentation of the brain into different nerve tracts.

The data set used in this thesis consisted of 63 SLE patients and 20 healthy controls. Previous analysis on this data set was limited to three nerve tracts because of time-consuming manual work of the segmentation. The aim of this thesis was to extend the analysis of the white matter microstructure to include all the major nerve tracts of the brain and by that, enable group-comparisons of the whole brain. This was done by implementing the methods into a pipeline where no manual work was required. Group comparison based on the extracted values was done between healthy controls and SLE patients and between the two classifications of the disease.

Significant differences of the microstructure were found when comparing SLE patients with healthy controls. In the comparison between the subgroups of SLE, with and without neuropsychiatric symptoms, the difference was not significant. This emphasizes the theory of the brain being affected in all SLE patients, and not only the ones having neuropsychiatric symptoms. The conclusion of this thesis is that the use of automated methods for extracting values of the white matter microstructure is a time-effective approach on analysis of large data sets, but it requires extensive quality control of each step.

Acknowledgements

This master's thesis was the final step for me to receive a Master of Science degree within Biomedical Engineering at the Faculty of Engineering LTH, Lund University. The work was done in the MR Physics Group, a research group in the Department of Medical Radiation Physics at Lund University, and lasted from January 2020 to June 2020.

The work of this thesis could not have been possible without help from others and I would like to express my appreciation to all persons helping me along the way. A special thanks to my supervisor Markus Nilsson. Thank you for always helping me forward when I was lost and for giving me new ideas and knowledge within many areas.

I would also like to thank Evgenios Kornaropoulos, one of the researchers that constructed the pipeline used in this thesis. Thank you for letting me use the pipeline and for all the hours you spent helping me to solve my computer problems.

A warm thanks to each and every one in the MR Physics Group for your warm welcoming to the group and for all the valuable feedback during the process of my work.

Last but not least, I would like to thank my friends and family for your endless love and support during this thesis and during all the years of my education.

Anna Wikström, June 2020

Abbreviations

2D	Two-dimensional
3D	Three-dimensional
CNS	Central Nervous System
CSD	Constrained Spherical Deconvolution
DKI	Diffusion Kurtosis Imaging
dMRI	Diffusion Magnetic Resonance Imaging
DTI	Diffusion Tensor Imaging
FA	Fractional Anisotropy
FCNN	Convolutional Neural Network
fODF	Fiber Orientational Distribution Function
HC	Healthy Control
MD	Mean Diffusivity
MK	Mean Kurtosis
MRI	Magnetic Resonance Imaging
NPSLE	Neuropsychiatric Systemic Lupus Erythematosus
PCA	Principal Component Analysis

RF Radio Frequency

ROI Region of Interest

SLE Systemic Lupus Erythematosus

Contents

Chapter 1
Introduction

1.1 Background

Systemic Lupus Erythematosus, SLE, is a chronic autoimmune disease with a large variation of symptoms. The central nervous system can be affected by the disease and some patients have neuropsychiatric symptoms. There are ways to classify the patients into neuropsychological SLE, NPSLE, and non-NPSLE, where no neuropsychiatric symptoms are present. One of the challenges in the classification is to determine if the symptoms that occur are connected to the disease or if it is due to other causes [1]. By studying the white matter microstructure in SLE patients and making comparisons with healthy controls, the disease and the neuropsychiatric symptoms can be better understood.

Magnetic resonance imaging, MRI, is a commonly used imaging technique when the brain is to be studied. It has the advantage of being able to image soft tissue and hence, the gray and white matter can be separated. To retrieve information about the microstructure of the white matter, diffusion MRI is needed. It measures the amount of diffusion of water molecules in the brain and based on this, the microstructure can be described. The use of diffusion MRI in clinical application started off with the use of detection of acute stroke in in end of the 20th century [2]. Later on, it has been used in a large variation of diseases, multiple sclerosis and brain tumors as an example [3, 4].

Segmentation of the white matter facilitates the comparison of microstructure in different parts of the brain. Diffusion MRI enables this segmentation of the brain into the different nerve tracts, which are bundles of nerve fibers with a specific function. Based on this segmentation, values can be extracted and analyzed between different groups of individuals. Segmentation of nerve tracts can be done manually but it is time-consuming and will restrict the analysis to a limited number of tracts.

Several studies have been done comparing the white matter microstructure in SLE patients. A study published by Nystedt et. al. showed that differences could be identified between healthy controls and SLE patients in some nerve tracts, but no differences were found between NPSLE and non-NPSLE patients [5]. Only three tracts were studied, which may give a biased view of which areas are affected by the disease. Analyzing all of the major nerve tracts of the brain could give a better understanding of the disease.

1.2 Aim and Problem Formulation

The data from the study published by Nystedt et al. [5] is used in this thesis. The aim of this thesis was to extend the analysis of the white matter microstructure to include all the major nerve tracts of the brain and by that, enable group-comparisons of the whole brain. The work could be divided into three different tasks:

1. Identify and implement a method that segments the major nerve tracts of the brain without demanding time-consuming manual work.

2. Validate the chosen method and investigate the statistical power of using different parameters to describe the microstructure.

3. Perform a statistical analysis on the values extracted by the method to gain new insights about SLE as a disease.

Segmentation of the brain is a time-consuming task and can limit the analysis to only include a subpart of the nerve tracts of the brain. To be able to study the whole brain, there is a need to use automated methods for the segmentation. The automated methods should be implemented in a pipeline to achieve a fully automated analysis of the brain.

In group-comparisons, the statistical power is important to consider. The statistical power is the probability of correctly rejecting a null hypothesis. If there is a difference between the two groups, the method should be able to find it. Different parameters should be investigated to achieve the highest statistical power.

There are several important research questions that needs to be answered to get a better understanding of SLE as a disease. This thesis aimed to answer three of these research questions:

- Are there any microstructural differences of the brain between patients with SLE and healthy controls?

- Are there any microstructural differences of the brain between SLE patients classified with NPSLE and the patients with non-NPSLE?
- What areas of the white matter in the brain are affected by the disease?

Chapter 2
Theory

2.1 Systemic Lupus Erythematosus

Systemic Lupus Erythematosus, SLE, is a chronic autoimmune disease. The prevalence of SLE was 60-70 cases/100 000 habitants in Sweden year 2016. The disease is more common in females and in the childbearing ages, the risk for women to develop SLE is 20 times higher than for men in the same age [6]. SLE appears in a remitting-relapsing manner; periods with a more active disease are alternated with periods of little or no evidence of the disease. SLE affects multiple organ systems, and many different symptoms may be observed. According to a study made on 1000 SLE patients published in 2009, the most common symptoms are arthritis, malar rash (facial rashes), and nephropathy (damage of the kidneys) [7].

The central nervous system can also be affected, which can lead to neuropsychiatric symptoms with a large diversity. It ranges from milder symptoms as headache, mood disorders, fatigue, and cognitive dysfunction to more severe symptoms as epilepsy, stroke, and psychosis. Different suggestions have been made on how to classify the disease in having neuropsychiatric symptoms or not. In 1999, The American College of Rheumatology presented 19 case definitions to achieve a standard way of diagnosing SLE patients in NPSLE, with neuropsychiatric symptoms, and non-NPSLE, without neuropsychiatric symptoms. The diverse symptoms make it hard to classify [8]. The neuropsychiatric symptoms may be a direct cause of the disease but might as well occur due to other reasons; side effects of medication or hypertension. The classification is even harder to make since many of these neuropsychiatric symptoms are common in all SLE patients and in the general population [6].

2.2 The Brain

The brain is one part of the central nervous system. The nervous tissue contains different types of cells where neurons are one of these. Neurons are the cells responsible for the communication and transmission of nerve signals. It consists of a cell body, dendrites that receives information and the axon that connects the neuron with the target. The axon is a long cylinder covered in myelin sheaths to make the transmission of the nerve signal faster [9].

A bundle of axons found in the central nervous system is called a nerve tract. In the brain there are several nerve tracts where each one has a specific function of transmitting signal and connecting different parts of the brain. Some nerve tracts are more involved in the cognitive tasks and memory, while other tracts are involved in the motor control of the body.

The nervous tissue of the brain can be divided into gray matter and white matter. The gray matter primarily consists of cell bodies and dendrites and the white matter are regions with many axons. It appears white because of the myelin that is a lipid-rich substance. In Figure 2.1, an MRI image of the brain can be seen showing the gray and white matter. Diseases affecting the brain may lead to minor deviations of the white matter microstructure. These deviations can be neuronal dead or a lower amount of myelin covering the axons.

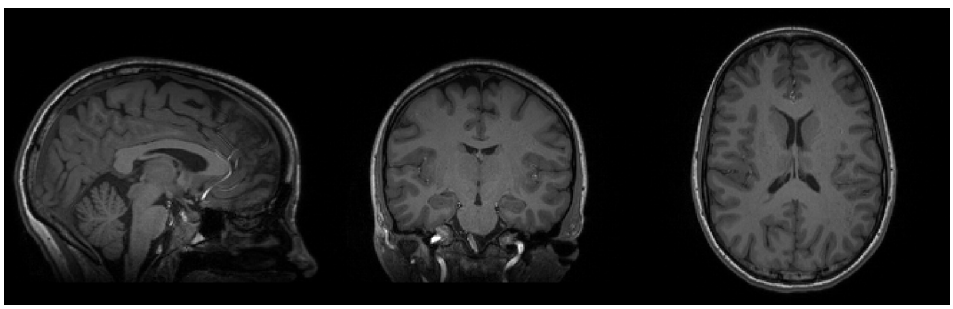

Figure 2.1: Example of an MRI image of the brain. The lighter parts of the brain are white matter and the darker areas on the peripheral parts of the brain are gray matter.

2.3 Magnetic Resonance Imaging

Magnetic Resonance Imaging, MRI, is an imaging technology that does not use any ionizing radiation. Compared to other imaging technologies, soft tissue is

better seen in MRI images. For instance, the gray matter and the white matter can be separated as in Figure 2.1.

It is the nucleus of the of the hydrogen atom, the proton, that makes MRI possible. The human body consists to a large extension of hydrogen, mainly in the form of water and fat. The proton has a spin, it rotates around its own axis. A nuclear magnetic moment appears in each proton, due to the fact that the proton is positively charged and that it rotates. The magnetic moment can be thought of as each proton being a small magnet. All the protons are randomly oriented in the absence of an external magnetic field, as can be seen in Figure 2.2a. To be able to construct a 3D image, the object being imaged will be divided into small volume compartments called voxels. All the protons placed within a voxel can be represented by a net magnetization vector by adding all the magnets, the protons, together. It is the net magnetization vector of each vector that is measured during an MRI acquisition.

When the human body is placed within an external magnetic field, the protons will change their direction and will start to precess. Instead of being randomly oriented, each proton will be parallel or anti-parallel to the direction of the external magnetic field, see Figure 2.2b. It is a slightly higher probability for the proton being in parallel because of the lower energy state. This leads to a greater number of protons aligned in that direction. The net magnetization of all the protons will have the same direction as the external magnetic field, the z-direction. The precession of the protons makes rotate around the z-axis in a wobbling motion. The frequency of the precession is called the Larmor frequency, and it is linearly proportional to the strength of the external magnetic field. The protons within a voxel do not precess in phase with each other, and the net magnetization vector can be viewed as non-rotating.

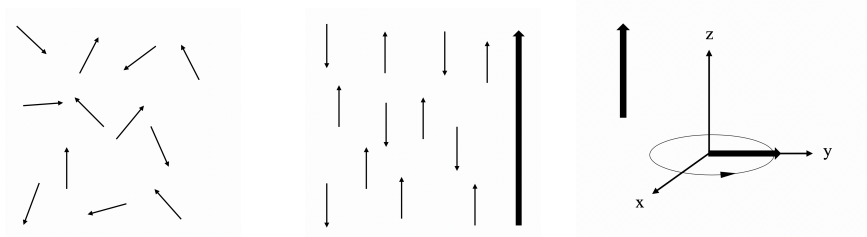

(a) The protons are randomly oriented in the absence of an external magnetic field.

(b) The protons align parallel or anti-parallel to the external magnetic field.

(c) After the 90°RF-pulse, the net magnetization vector is directed in the x-y-plane.

Figure 2.2: The basics for MRI technology.

The use of radio frequency pulses, RF-pulses, is an important step in the MRI acquisition. An RF-pulse is applied with the Larmor frequency causing the protons to absorb this energy. The energy absorption makes the protons precess in phase with each other and the direction will be flipped 90°, causing the net magnetization to be oriented in the x-y-plane. Since the protons are precessing in phase, the net magnetization vector will rotate around the z-axis. A schematic explanation of the net magnetization vector after the RF-pulse can be seen in Figure 2.2c. The rotation of the net magnetization vector is measured in the MR scanner by the use of receiver coils.

Two things will appear after the 90°RF-pulse; change of direction and dephasing. The direction of each proton will return back to the direction of the external magnetic field. The protons will also dephase due to the slightly different frequencies of their precession, causing the net magnetization vector to be smaller as can be seen in Figure 2.3a. How fast the dephasing and direction change will occur is due to the tissue characteristics and that is why different tissues can be visualized with MRI.

The dephasing of the protons can be reversed by the use of a second RF-pulse. The protons are flipped 180-degrees in the x-y-plane causing the dephasing to be reversed, see Figure 2.3b. By the time for readout, the protons will precess in phase again and the net magnetization vector is maximized in the x-y-direction. The effect of the dephasing will be removed, and it is mainly the change of the protons directions that will be imaged. The process of the dephasing and the use of the 180°RF-pulse is described in Figure 2.3.

Field gradients are applied to enable the spatial encoding of the signal. Field gradients in x-, y-, and z-direction change the magnetic field that each voxel is af-

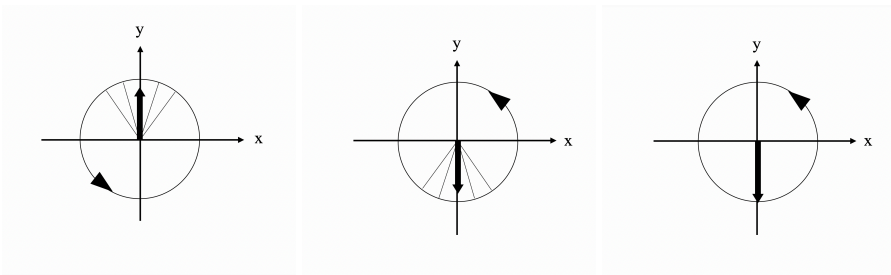

(a) The protons will dephase, making the net magnetization vector smaller.

(b) After the 180°RF-pulse, the protons will change their direction again.

(c) The spins will precess in phase and by the time for readout.

Figure 2.3: Dephasing of the protons.

fected by. The gradients are applied in different time points during the acquisition, causing the protons to be affected by different strengths of the external magnetic field. The image is reconstructed by using the Fourier transform of the k-space that is created for each slice. The k-space includes information about phase, frequency and intensity for the different voxels in that slice.

2.4 Diffusion MRI

In diffusion MRI, the diffusion of water molecules is measured and can be used to estimate characteristics of the microstructures in the brain. Diffusion is the random movement of molecules due to thermal energy. The mean-square displacement of a molecule in three dimensions, $\langle r^2 \rangle$, can be described by

$$\langle r^2 \rangle = 6Dt$$

where D is the diffusion coefficient and t is the diffusion time. The diffusion coefficient in liquids depends on the temperature and characteristics of the material.

In a large gathering of water, the diffusion is isotropic. It means that the probability for a molecule to diffuse is the same in all directions. In the brain there are several structures restricting the diffusion of water molecules. The diffusion is not the same in every direction and it is therefore said to be anisotropic. One of the structures restricting the diffusion is the myelinated axon. The diffusion is not restricted along the axonal direction whereas perpendicular to the direction of the axon, the diffusion is restricted due to the cell membrane and the myelin sheaths. The water molecules will diffuse to a larger extent in the axonal direction than perpendicular to it.

The basics for the technique behind diffusion MRI were introduced by Stejskal and Tanner in 1965 [10]. A specific MRI sequence with two diffusion gradients enables the measuring of the diffusion, the principle for the sequence can be seen in Figure 2.4. The first diffusion gradient leads to a phase shift among the protons in the gradient direction. The protons will continue their dephasing and will also move due to the diffusion. The 180-degree RF-pulse will revert the dephasing of the protons. The second diffusion gradient induces a phase shift opposite to the first gradient. The protons that have diffused between the two gradients will experience unequal effects by these and will not have completely rephased by the time for readout. This leads to a signal loss where higher signal loss is an indication of larger amount of diffusion.

During the acquisition, the signal is measured with and without the use of diffusion gradients. The diffusion gradients are applied in several directions to be

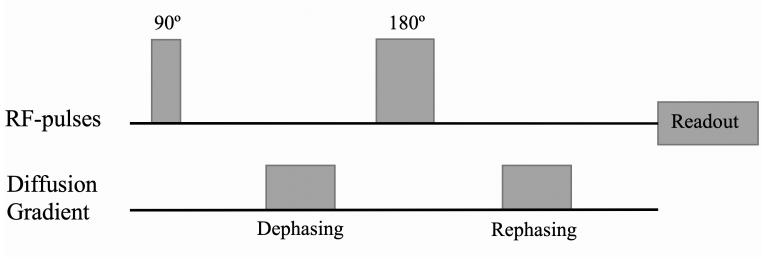

Figure 2.4: Schematic image of the MRI sequence used for diffusion MRI.

able to model the diffusion of molecules in different directions. The characteristics of the diffusion gradients, strength, duration, and spacing of the gradients, are represented by the b-value. The direction of the gradient is given by the b-vector. The measured signal, the b-values, and the b-vectors are used to model the diffusion. There are several different techniques for the acquisition of diffusion MRI where Diffusion Tensor Imaging, DTI, and Diffusion Kurtosis imaging, DKI, are examples of these.

2.4.1 Diffusion Tensor Imaging

One way to model the diffusion in each voxel is to use the diffusion tensor, which is the basis for Diffusion Tensor Imaging, DTI [11]. The signal with the diffusion gradient explained by b can be modeled as

$$S(b) = S(0)e^{-bD}$$

where $S(0)$ is the signal without diffusion gradients and D is the diffusion coefficient. The diffusion is assumed to be Gaussian, but the variance of the diffusion is different in spatial directions. Since the diffusion is not isotropic in the brain, the diffusion coefficient D must be explained in a different way than only with a scalar. The diffusion tensor is a 3 x 3 matrix given by

$$\mathbf{D} = \begin{bmatrix} D_{xx} & D_{xy} & D_{xz} \\ D_{yx} & D_{yy} & D_{yz} \\ D_{zx} & D_{zy} & D_{zz} \end{bmatrix}$$

where D_{ab} describes the diffusion in the direction from a to b. Since the diffusion is the same in the direction a to b as in b to a, $D_{ab} = D_{ba}$, **D** is a real and symmetric matrix. By the use of single value decomposition, the tensor **D** can be explained by its eigenvalues and eigenvectors. The geometrical representation of

the diffusion tensor is an ellipsoid rotated in the direction of the eigenvectors and the eigenvalues describes the shape. The tensor can be seen in Figure 2.5 where λ_1 is the largest eigenvalue and thus represents the principal direction of diffusion.

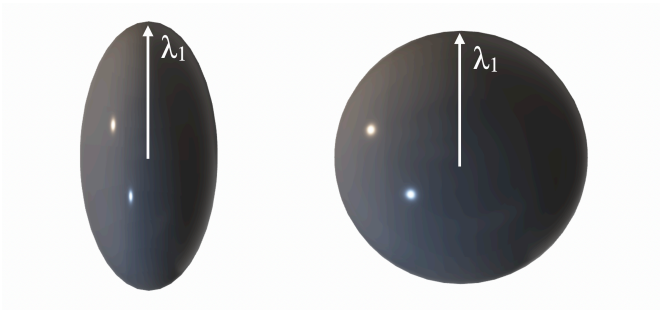

Figure 2.5: Schematic image of two different diffusion tensors. The tensor to the left is anisotropic, and the principal direction of the diffusion is pointed out by the arrow representing the first eigenvalue λ_1. The tensor to the right is isotropic, and it can be represented as a sphere.

The eigenvalues are used to represent the diffusion with different parameters. The mean diffusivity, MD, and the fractional anisotropy, FA, are calculated as

$$MD = \frac{\lambda_1 + \lambda_2 + \lambda_3}{3}$$

and

$$FA = \sqrt{\frac{(\lambda_1 - \lambda_2)^2 + (\lambda_2 - \lambda_3)^2 + (\lambda_3 - \lambda_1)^2}{2(\lambda_1^2 + \lambda_2^2 + \lambda_3^2)}}.$$

MD is the mean of all eigenvalues and gives a measure of the displacement of the water molecules. FA is the variance of the eigenvalues and gives a relative measure of the anisotropy. It ranges from 0 to 1 where $FA = 0$ means that the diffusion is isotropic, all eigenvalues are equal and the tensor is represented as a sphere, as the right part of Figure 2.5. Larger values of FA mean that the diffusion is anisotropic, and the diffusion has a principal direction. The fractional anisotropy can also be interpreted as the fraction of diffusion that is present in the predominant direction of diffusion. With high values of FA and low values of MD, the white matter is indicated to be intact. A lowered FA and increased MD could be an indication of tissue damage of the white matter.

2.4.2 Diffusion Kurtosis Imaging, DKI

Diffusion Kurtosis Imaging, DKI, is an extension of the DTI model and without the assumption about the distribution being Gaussian [12]. DKI gives the possibility to quantify the non-Gaussianity of the diffusion. The tensor model is complemented with the kurtosis parameter, which is a parameter describing the peakedness of a distribution. The equation describing the signal loss is given by

$$\ln \frac{S(b)}{S(0)} \approx -bD + \frac{1}{6}b^2(MD)^2MK$$

where MD is the mean diffusivity and MK is the mean kurtosis. It is the average of the kurtosis among all directions. A higher value of the kurtosis means that the diffusion is more restricted. It gives a hint that the environment is more complex and that it does not follow a Gaussian distribution [13]. The kurtosis parameters are more sensitive to heterogeneity of the diffusion in neural tissue [14].

To be able to model the diffusion by DKI, another acquisition technique is needed than for the DTI. It requires at least three different b-values and a larger number of directions of the gradients than is needed for the acquisition of DTI.

2.4.3 Constrained Spherical Deconvolution, CSD

The diffusion tensor model is valid in voxels with one main direction of the diffusion. In case of a voxel where several nerve bundles pass by, and with different directions, the diffusion tensor model is not sufficient. With constrained spherical deconvolution, CSD, the diffusion can be modeled in several directions.

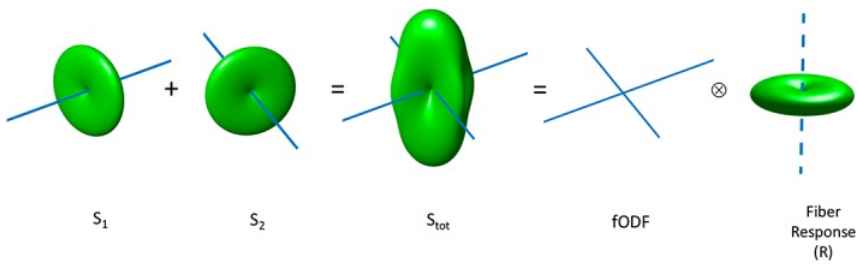

Figure 2.6: The principle of constrained spherical deconvolution. S_{tot} is the measured signal, it is modeled as the sum of two separate signals, S_1 and S_2, from two fibers with different directions. The direction of the fibers, fODF, can be achieved by deconvolving S_{tot} with the response function. Source: Figure from [15].

The principle of this model can be seen in Figure 2.6. The total measured signal in each voxel, S_{tot}, is the sum of contribution from several different fibers. This can be modeled as the convolution of the orientational distribution function of the fibers, fODF, with the response function R that explains the signal contribution from one fiber. It is the fODF that is of interest, which can be achieved by spherical deconvolution of S_{tot} with the fiber response [16]. Since deconvolution is sensitive to noise, the robustness of the method is achieved by the constraint of only accepting non-negative values [17].

2.4.4 Tractography

Diffusion MRI, and especially the use of CSD, enables information about the direction (or directions) of the diffusion in each voxel. The direction of the diffusion is expected to correspond to the direction of the axons in the brain. Tractography uses the directional information to reconstruct the pathways of the white matter. Streamlines are estimated by following the main diffusion direction of adjacent voxels, it tracks the path where the diffusion is least hindered. A map with the streamlines calculated by the tractography is called a tractogram, see an example in Figure 2.7. The streamlines will be an assumption of how the fiber bundles, a gathering of axons, are oriented in the brain. The tractogram gives an estimation of the network of nerve fibers within the brain. Tractography can also be used in order to segment different nerve tracts of the brain.

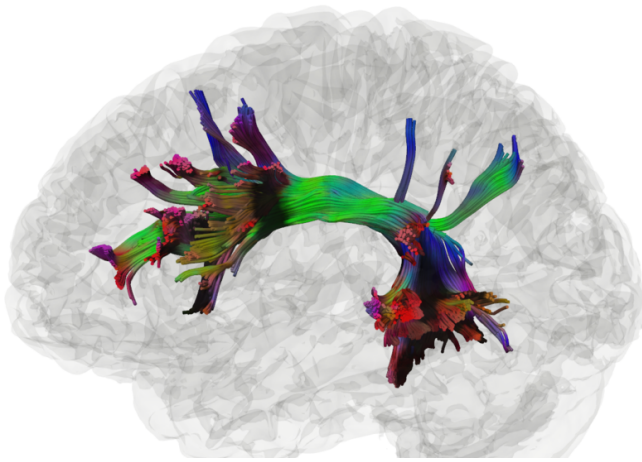

Figure 2.7: Streamlines after calculated tractography in a part the brain. Source: Figure from [18].

2.4.5 Gradient Directions

Some applications of the diffusion MRI require that the spatial information and the orientational information in each voxel are represented in the same coordinate system. The scanner, the imaging protocol, and the software used to process the images might have different coordinate conventions. The directional information about the diffusion is extracted based on the representation of the coordinate system of the b-vectors, which are the gradient directions. If the processing software expects a different representation of the coordinate system than the existing, the directional information about the diffusion will be wrongly oriented. Correct representation of the gradient directions can be achieved by permutation of the axes, changing the order of x, y, and z, and/or change the polarity of one axis [19].

Tractography is dependent on the estimated direction of the diffusion since the streamlines follow the main direction of the diffusion. In case of estimating fODFs on wrongly oriented gradient directions, as can be seen in the left part of Figure 2.8, the streamlines will not follow the nerve tract as expected. When the gradient directions are correct, as can be seen in the right part of Figure 2.8, the estimated streamlines will be as expected.

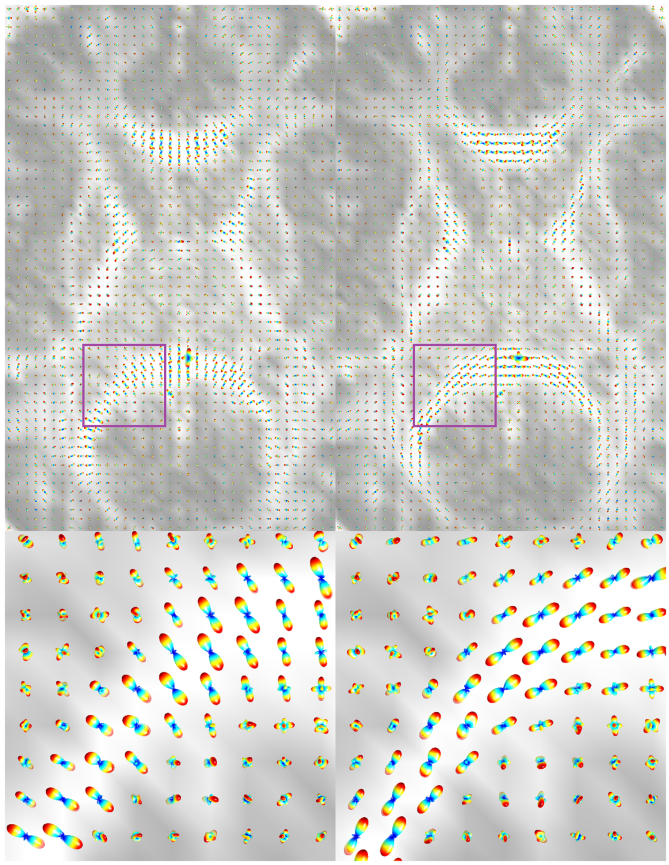

Figure 2.8: Showing the problems with gradient directions, where the fODFs are overlaid on the FA map. Left: the fODFs are reconstructed based on the original gradient directions. Right: the fODFs after correction of the gradient directions. Source: Figure from [19]

2.5 Segmentation of Nerve Tracts

As explained in Section 2.2, the bundles of axons in the brain can be categorized into different nerve tracts. To extract information about the diffusion within one tract, segmentation of the brain into the different nerve tracts is required. The basic idea behind the segmentation is that the tractogram of the whole brain is calculated. The tractogram can be segmented into different tracts by determining which of the streamlines that belong to a specific tract. This can be achieved in different ways, manually or automated.

Manual segmentation of the nerve tracts requires someone to draw regions-of-interests, ROIs, in each individual. The ROIs for each tract are placed in the anatomical regions known to be a part of that tract. All streamlines passing through the ROIs will be the segmentation for that tract. The manual drawing of ROIs in each individual can induce variability of the segmentation, which might reduce the statistical power in comparison between individuals. Another drawback with manual segmentation is that it is time-consuming and hence, might limit the analysis of nerve tracts to only include a few nerve tracts of the brain.

In order to reduce the need of manual work for the segmentation, different methods have been published that does the segmentation in a more automated way. The automated segmentation methods could be categorized into three groups:

- ROI-based segmentation
- Clustering-based segmentation
- Direct segmentation

The ROI-based segmentation uses Regions of Interests, ROIs, to achieve the segmentations. The ROIs could be gathered from different atlases, where the regions are pointed out in a standard brain. The ROIs from the atlases will be registered to the individual space, projecting the ROIs on the brain to be segmented. The tractograms are filtered through the ROIs, and the streamlines that runs through the ROIs for that specific tract is segmented. This method requires the tractogram of the brain and will also be in need of registration of images from one space to another.

The clustering-based segmentation is about grouping the streamlines into clusters. The clustering could be done manually or automatically by the use of an atlas and will then be assigned to a specific nerve tract. This method also requires the tractogram of the brain.

The direct segmentation is different than the other techniques. It is named direct because the segmentation is done without the use of calculating the tractogram. Tractography is time-consuming and computer power demanding. By skipping the step of calculating the tractogram of the brain, the segmentation could be achieved faster. Several methods of direct segmentation are available, using mathematical models or deep learning approaches to go from the input dMRI image to segmentation of the nerve tracts [20, 21].

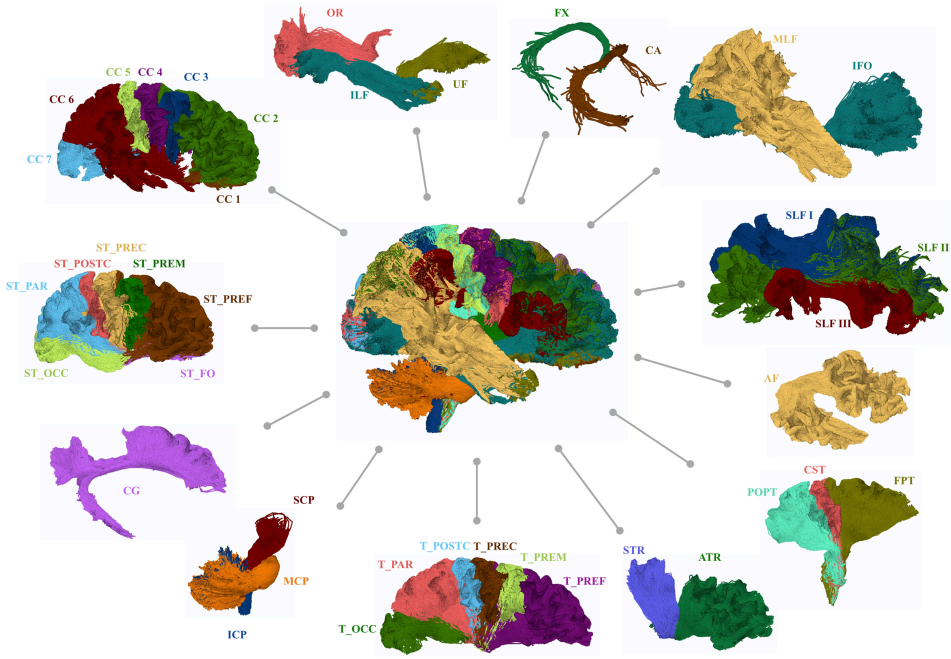

Figure 2.9: Nerve tracts segmented by TractSeg. Source: Figure from [20]

2.5.1 TractSeg

TractSeg is one of the published methods using the approach of a direct segmentation. It is a method implemented in Python and available as an open-source package. The method was developed by Wasserthal et. al. in Heidelberg, Germany [20]. The segmentation does not require tractography but is instead based on deep leaning. The input to the method is a dMRI image with corresponding b-values and b-vectors and the output is binary segmentations of 72 different nerve tracts.

Several steps are implemented in the method, which can be seen in Figure 2.10. The first step of TractSeg is preprocessing. Based on the dMRI image, b-values, and b-vectors, the fiber orientations are calculated by the use of constrained spherical deconvolution. Based on the fiber orientations, the three main directions of the diffusion in each voxel are extracted as the peaks. The next step of the method utilizes deep leaning, more specifically fully convolutional neural networks, FCNNs. The FCNNs use the peaks as input and outputs a binary 3D image for each of the 72 nerve tracts. In the 3D image for one tract, the voxels with a value of 1 will have a probability higher than 0.5 that the tract passes through that voxel.

When using TractSeg, the parameters for the FCNNs are pretrained. During the training of the network, heavy data augmentation was used in order to make the method robust for different input images. The augmentation included different rotations of the brain, elastic deformation, displacement of the brain, zooming, resampling to mimic lower resolution, Gaussian noise, and different contrast and brightness of the image.

In the publication of the method, TractSeg is compared with six other methods for segmentation of nerve tracts. In the comparison, the method was found to be up to 535 times faster than the average of the other methods. By comparing the overlap of the segmentations of the different methods with a ground truth created by the same authors, the segmentation based on TractSeg had the highest overlap in all tracts. The authors states that TractSeg outperforms the other methods when comparing the segmentations and with one advantage of being much faster than the other methods.

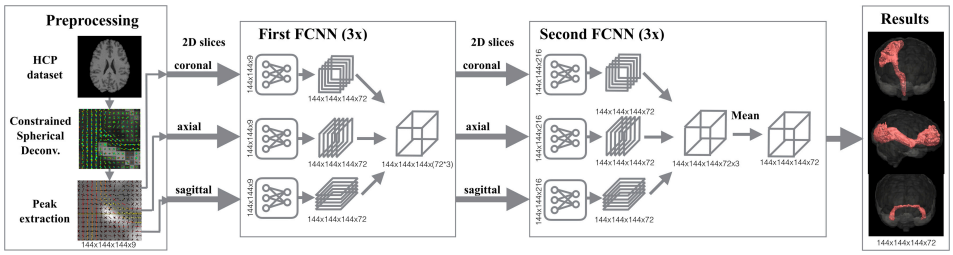

Figure 2.10: Processing steps for TractSeg. Source: Figure from [20]

2.6 Statistical Power

Group-comparisons are commonly done by the use of a statistical test. The statistical power of a test can be explained as the probability of rejecting the null hypothesis when it is false. This can be interpreted as the probability to find the difference between two groups, if there is a difference to be found. Statistical power can be used to determine the sample size for a planned study but can also be used to evaluate results.

The power of a statistical test is related to several parameters; the significance level, the effect size and the sample size. By keeping the significance level and the sample size constant, the effect size could be investigated on two different methods to be able to compare their statistical power. Larger effect size means higher statistical power and indicates higher probability of finding differences.

2.6.1 Effect Size

Effect size is a quantitative measure explaining the magnitude of the effect when doing group comparisons. In case of group comparison where the mean value of each group is compared, the effect size gives a measure of how well separated the mean values are and if it is possible to detect the difference. The effect size is a complement to the significance of a statistical test, since it can tell how large the difference is between the two groups. Comparing different parts of the brain, the effect size will tell where the largest difference appears. Comparing different methods, the effect size will give an indication on which of the studied methods that gives the highest probability of finding the difference.

Several metrics are available to define the effect size of a test. When the test is based on comparing the difference in means of two groups, Cohen's d is a common metric [22]. It is defined by

$$d = \frac{\mu_1 - \mu_2}{s},$$

where μ_1 and μ_2 are the means of the two populations and s is the pooled standard deviation. The pooled standard deviation is defined by

$$s = \sqrt{\frac{(n_1 - 1)s_1^2 + (n_2 - 1)s_2^2}{n_1 + n_2 - 2}}$$

where n_1 and n_2 are the number of individuals and s_1 and s_2 are the standard deviations in each population. Examples of different values of Cohen's d can be seen in Figure 2.11. The effect size is defined to be small if $d = 0.2$, where it is almost impossible to see a difference between the groups. A medium effect size is achieved if $d = 0.5$, where the difference between the two group-means are large enough to be visible. The effect size is defined to be large when $d = 0.8$.

In the development of a methodology, it is important to take effect size into consideration. The effect size is lowered when the standard deviation is increased. The method should restrict the amount of induced variance in order to keep the effect size high.

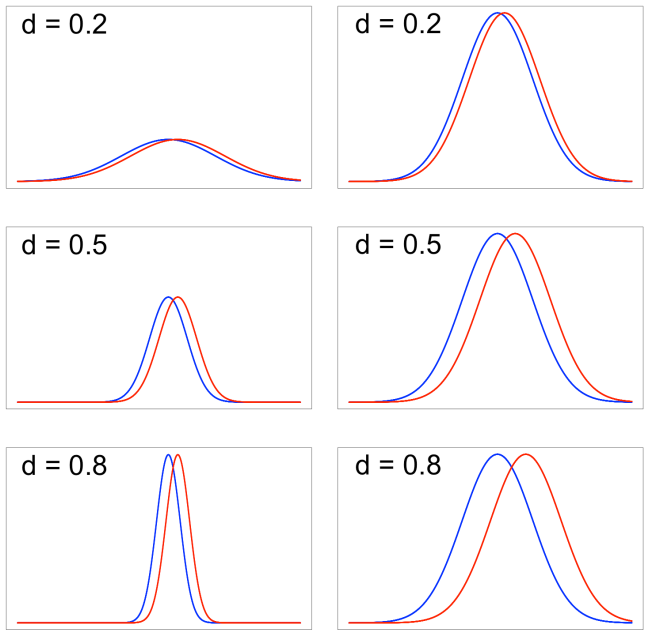

Figure 2.11: Plot over Cohen's d. In the left column, the difference between means are constant and d becomes larger when the standard deviation s is decreased. To the right, the standard deviation s is kept constant and it can be seen that d increases with an increase in the difference between the two means.

Chapter 3
Data

The diffusion MRI images used in this thesis were gathered in a study of SLE patients [5]. The study contained patients diagnosed with SLE, both NPSLE and non-NPSLE, as well as healthy controls. Due to the fact that SLE is more commonly found in females, the study only consisted of women. All individuals went through a cognitive test, blood test and were scanned in the same 3T MRI scanner. Diffusion MRI images of each individual were gathered with DKI and DTI resulting in two data sets measuring the diffusion of the brain. These two techniques are using different MRI sequences during the acquisition, see Section 2.4 for detailed information about the acquisition techniques. One major difference between the two data sets is the difference in resolution. The DTI data has better resolution, smaller voxel size, than the DKI data as can be seen in Table 3.1.

The study consisted of 71 patients with SLE and 25 healthy controls. Some SLE patients were excluded due to left-handedness or not being able to fulfill the MRI. Some healthy controls were excluded for invalid cognitive testing and dyslexia. The final set-up used in this thesis is 20 healthy controls and 63 SLE patients. The number of individuals in each group, and their age can be seen in Table 3.2.

Table 3.1: Resolution of the different data acquisitions

	Voxel size
DKI	2,3 x 2,3 x 2,3 mm^3
DTI	2,0 x 2,0 x 2,0 mm^3

Table 3.2: Number of participants for the three different groups and their age.

	Individuals	**Age**
HC	20	36 (23 - 52) years
NPSLE	37	37 (18 - 49) years
non-NPSLE	26	35 (18 - 51) years

Chapter 4
Method

This chapter cover the methods used in this thesis. A major part of the work consisted of development and validation of a methodology to extract parameters that can be used for group-comparison. To facilitate the reading and understanding of the methodology, some results from the development of the methodology are presented in this chapter. The chapter starts with a description of the principle behind the method and the pipeline used. The following sections describe the four steps of the method, where an overview of the steps can be seen in Figure 4.1.

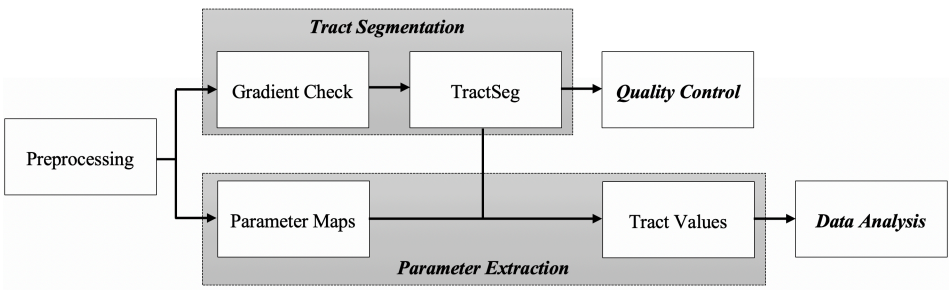

Figure 4.1: Flow diagram over the steps of the method

4.1 Pipeline

One of the tasks in this thesis was to develop an automated method that does not require any manual work on the segmentation of nerve tracts. In order to make the analysis automated, all the steps of the methodology except for the Data Analysis were implemented as nodes in a pipeline. The principle behind the use of a pipeline is that several methods are connected in a network where each method is called a

node. When the pipeline is running, it will run all the methods for each individual in that data set. The pipeline used in this work was constructed by the use of a python package called Nipype [23]. The existing pipeline included a lot of nodes, mainly preprocessing steps of the data to remove noise and motion artefacts. Since two different data sets were to be analyzed, two versions of the pipeline were constructed: DTI and DKI.

4.2 Tract Segmentation

4.2.1 Open-source methods

A literature survey was done to find how to do the segmentation of the nerve tracts in an automated way. In Section 2.5, the findings from the literature survey are summarized. Different methods were searched for, but two requisites were stated: the method must be Python-based and available open-source. The method needed to be implementable in Python to be able to include it in the pipeline.

TractSeg was found during the search for an automated method for the segmentation. It is a well-documented method implementable in Python and it has large benefit of having short running time. The paper presenting the method shows good results of the segmentation of nerve tracts using TractSeg in comparison to other state-of-the-art methods. The low running time and the sake that it was well documented was reason enough for it to be chosen as the method for segmentation.

4.2.2 Gradient Check

As explained in Section 2.4.5, some methods depend on that the coordinate systems of the gradient table and the background image are the same. TractSeg was shown to be dependent on these directions since the use of TractSeg without checking the gradient directions did not segment the nerve tracts correctly. The method chosen for the control of the gradient directions was *dwigradcheck* from the software MRTrix [24]. It runs through different combinations of directions of the b-vectors. For each combination, streamlines are calculated and summed. The output of the method is the rotated b-vectors in the direction with the largest sum of streamlines.

4.2.3 TractSeg

The diffusion MRI image with corresponding b-values and rotated b-vectors are inputs to TractSeg. Based on a convolutional neural network, the method calcu-

lates the binary segmentation of 72 different nerve tracts. The output from this step is 72 3D images for each individual. The segmentation process of TractSeg is explained further in Section 2.5.1.

4.3 Parameter Extraction

4.3.1 Parameter maps

The diffusion tensor and the kurtosis tensor were calculated to be able to extract parameters from these. The method DTIFIT from the software package FSL [25] was used to calculate the diffusion tensor based on the DTI data. DiffusionKurtosisModel, a method from the software package DIPY [26], was used for the DKI data. Before determining the kurtosis tensor, smoothing of the DKI data was needed. A Gaussian sphere with different values of the standard deviation, σ, was tested. One individual was used as a reference and it was determined to set the standard deviation to $\sigma = 0.75$.

Five parameter maps were determined for each individual; FA and MD based on the DTI data, and FA, MD, and MK based on the DKI data. An example of these parameter maps for one individual can be seen in Figure 4.2. The result of this step was 3D images where each voxel contains the value of the parameter in that voxel.

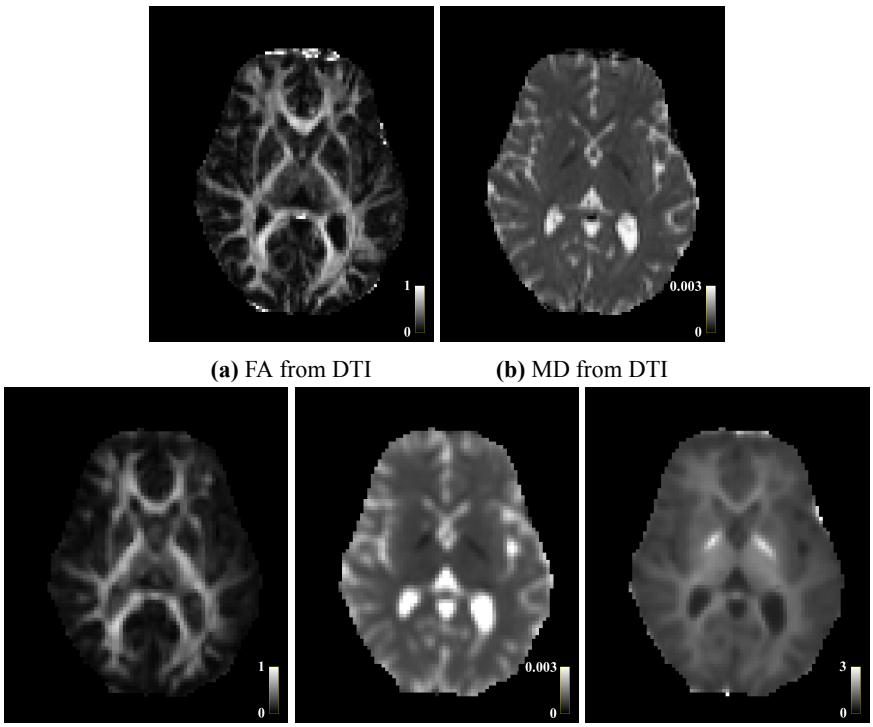

(a) FA from DTI **(b)** MD from DTI

(c) FA from DKI **(d)** MD from DKI **(e)** MK from DKI

Figure 4.2: The five different parameter maps from one individual. Note the different scaling of the intensity.

4.3.2 Tract Values

The nerve tract segmentations and the extracted parameters were combined to be able to represent each tract with one value. This was done by taking the mean value of the parameter in each tract. The volume for each tract was calculated to be used for quality control of the segmentations.

The output from the pipeline were seven different spreadsheets including information about all the 72 different tracts in the 83 individuals. The seven spreadsheets were:

- Mean FA from DTI
- Mean MD from DTI
- Volume based on DTI

- Mean FA from DKI
- Mean MK from DKI
- Volume based on DKI

4.4 Quality Control

With the output from the pipeline being a spreadsheet of values for each individual and tract, quality control was needed to validate every step of the pipeline. The quality control of the segmentation consisted of two different parts; visual inspection of the segmentations and investigation of the coefficient of variation for the volume for each tract.

The visual inspection of the tracts was enabled by the creation of a 2D image with all segmentations for one individual. 2D projections of all tracts were placed on top of the dMRI image. This image facilitated the quality control since the segmentations could be visualized.

The volumes were controlled to find the nerve tracts with a large variation in volume, which might be an indication that the segmentation was wrong for some individuals. The volume of each tract was normalized by the total brain volume for that individual to remove the variability of brain size between individuals. The coefficient of variation, C_v, was used to enable comparison of the variability in different tracts. It is defined as

$$C_v = \frac{\sigma}{\mu}$$

where σ is the standard deviation and μ is the mean value. A higher C_v indicates a larger variation of the volume among individuals for that tract.

The nerve tracts with the highest C_v was controlled by plotting the largest and the smallest volume for each tract. Large variations of the segmentations motivated the removal of six of the nerve tracts from further analysis. 72 tracts were segmented but the data analysis was only performed on 66 tracts after removal of the tracts with a large variation of the volume.

4.5 Data Analysis

All statistical analyses of the data were performed in RStudio [27]. The analysis started by controlling the normal distribution of all parameters. Then, the group comparisons were done and lastly, the effect size was evaluated on each comparison. The three steps are further explained in the following sections.

4.5.1 Control of Normal Distribution

Shapiro-Wilk test was used to control if the parameters were normally distributed within each group. It tests the null hypothesis that a sample came from a normally distributed population. A major part of the parameters from the DKI data were found not to be normally distributed. When plotting the distribution of the mean values of all individuals it was found that four individuals were outliers. These individuals had the largest (or smallest) mean values for all tracts. By studying the parameter maps of the outliers, it was found that one of the individuals had a distorted MK map, which can be seen in Figure 4.3. The raw images from the DKI of this individual showed that the patient had moved during the acquisition and the preprocessing in the pipeline could not remove the effect of the motion artefact. Due to the distorted input image this individual was removed from further analysis of the DKI data, but it was kept in the analysis of the DTI data. The other three individuals, that were found to be outliers, had slightly brighter (or darker) MK maps than the major part of the individuals. Since it was not certain that this was due to the anatomy or if the processing was wrong, these individuals were kept in the DKI analysis.

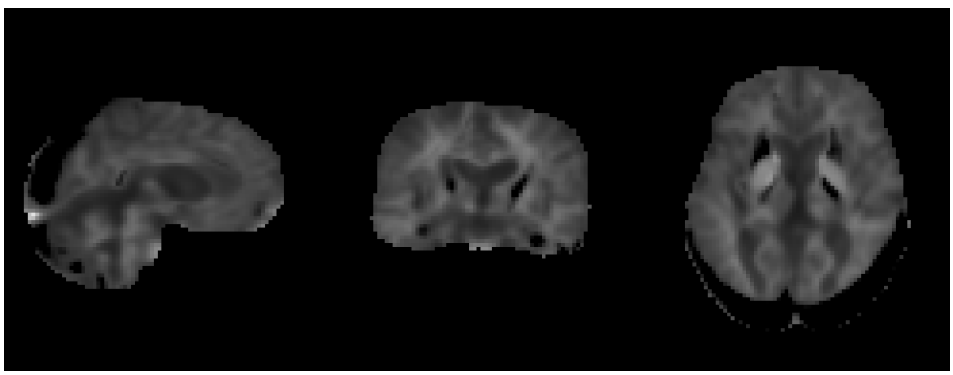

Figure 4.3: MK map of one of the individual removed from the DKI data.

4.5.2 Group Comparison

Two different group comparisons were done, comparing healthy controls with all SLE patients and comparing NPSLE patients with non-NPSLE patients. The comparison was done tract by tract, by the use of Welch's t-test, and with an attempt to include all tracts, by the use of principal component analysis.

Welch's t-test

Comparisons between the groups was done tract by tract to answer the question about which areas that are affected by the disease. Since the two groups did not have equal sample size and the variance could not be assumed to be equal, Welch's t-test was used. A test was done for each of the five different parameters, the 66 different segmented nerve tracts and for the two different group-comparisons. The t-statistics of the Welch's t-test is calculated as

$$t = \frac{\overline{X}_1 - \overline{X}_2}{\sqrt{\frac{s_1^2}{N_1} + \frac{s_2^2}{N_2}}}$$

where $\overline{X}_i$ is the mean value, s_i is the standard deviation and N_i is the sample size for population i. The p-value is calculated based on the t-statistics and the degrees of freedom. As an example, a two-sided null hypothesis was stated as

$$H_0 : \text{average of } \overline{MK}_{tract} \text{ for SLE} = \text{average of } \overline{MK}_{tract} \text{ for HC}$$

for each of the 66 tracts for the MK parameter in the comparison between SLE and healthy controls. The significance level was set to 0.05 without correction for multiple comparisons.

Multiple comparison problem

When doing multiple hypothesis tests on the same set of data, the significance level, σ, is valid for each test but does not cover all the comparisons. To avoid potential problems with analysis of multiple hypothesis tests on the same data set, the significance level needs to be lowered. This can be done by Bonferroni correction. The significance level is divided by the number of hypothesis tests that should be done. After Bonferroni correction, the significance level for each hypothesis test was determined to be

$$\frac{\sigma}{n} = \frac{0.05}{66} = 0.00076.$$

Principal component Analysis

The t-test done for each tract only tests if there is any difference between the two groups in that specific tract. To include all tracts in one test, principal component analysis was used. Principal component analysis, PCA, is a method that could be used for dimensionality reduction of data. It uses orthogonal linear transformations into a new coordinate system where the first coordinate explains most of the

variability in the data and the second one, the second most variability and so on. It is also a powerful tool for visualization of high-dimensional data. The data points for each parameter was plotted by the first two principal components. A Welch's t-test was also done on the first principal component.

4.5.3 Effect Size

Comparison of statistical power of the different parameters was enabled by calculating Cohen's d. The effect size was used to compare the statistical power and also to find the tracts that showed the largest effect of the difference between the groups. The theory behind effect size and Cohen's d is explained further in Section 2.6.

Chapter 5
Results

5.1 Pipeline

5.1.1 Quality Control

The pipeline run properly for the two data sets and values could be extracted from all individuals. The visual inspection of the segmentations did not find any wrongly segmented tracts. An example of an image from the visual inspection of the segmentation can be seen in Figure 5.1.

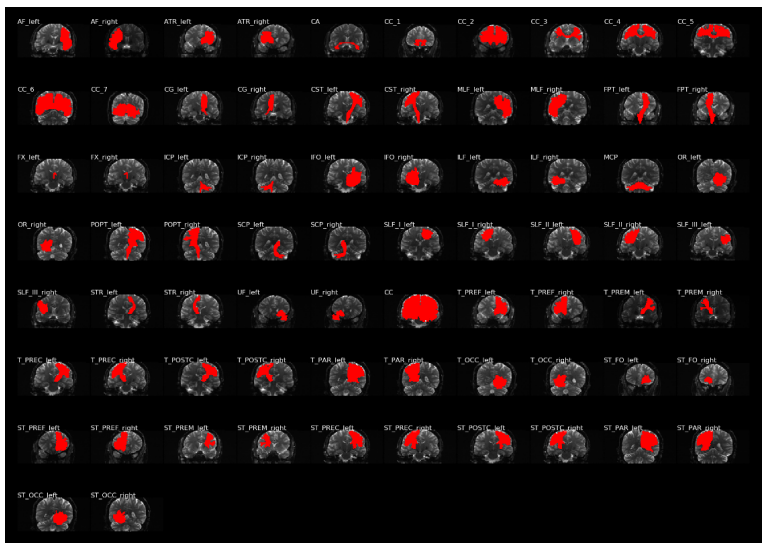

Figure 5.1: Image from the quality control. The segmentation of each tract is projected onto the diffusion MRI image of that individual.

The quality control of the coefficient of variation resulted in the removal of six tracts from further analysis. The coefficient of variation, C_v, for the normalized volume had similar values on the segmented tracts based on the DKI and the DTI data, which can be seen in Figure 5.3. The mean value of C_v for all tracts was 0.13 for both of the data sets. The standard deviation was larger for the DKI data, with $s = 0.045$, than for the DTI data, with $s = 0.040$.

The fornices, FX_left and FX_right, and the inferior and superior cerebellar peduncles, ICP_left, ICP_right, SCP_left, and SCP_right, were found to have C_v larger than 0.2. This means that the standard deviation covers more than 20% of the mean value. By plotting the highest and the lowest volume of these tracts and comparing these, it was found that the segmentation varied considerably as can be seen in Figure 5.2. Different areas of the tract are covered for each individual and hence, the group comparison in that tract will not be valid. These six tracts were removed from further analyses.

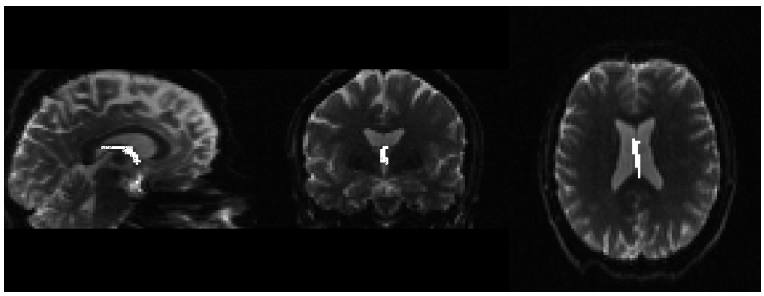

(a) Segmentation in the individual with the lowest volume.

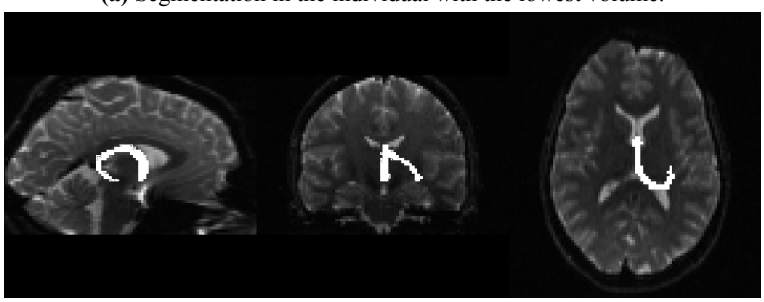

(b) Segmentation in the individual with the highest volume.

Figure 5.2: Comparison of the segmentation of the left fornix.

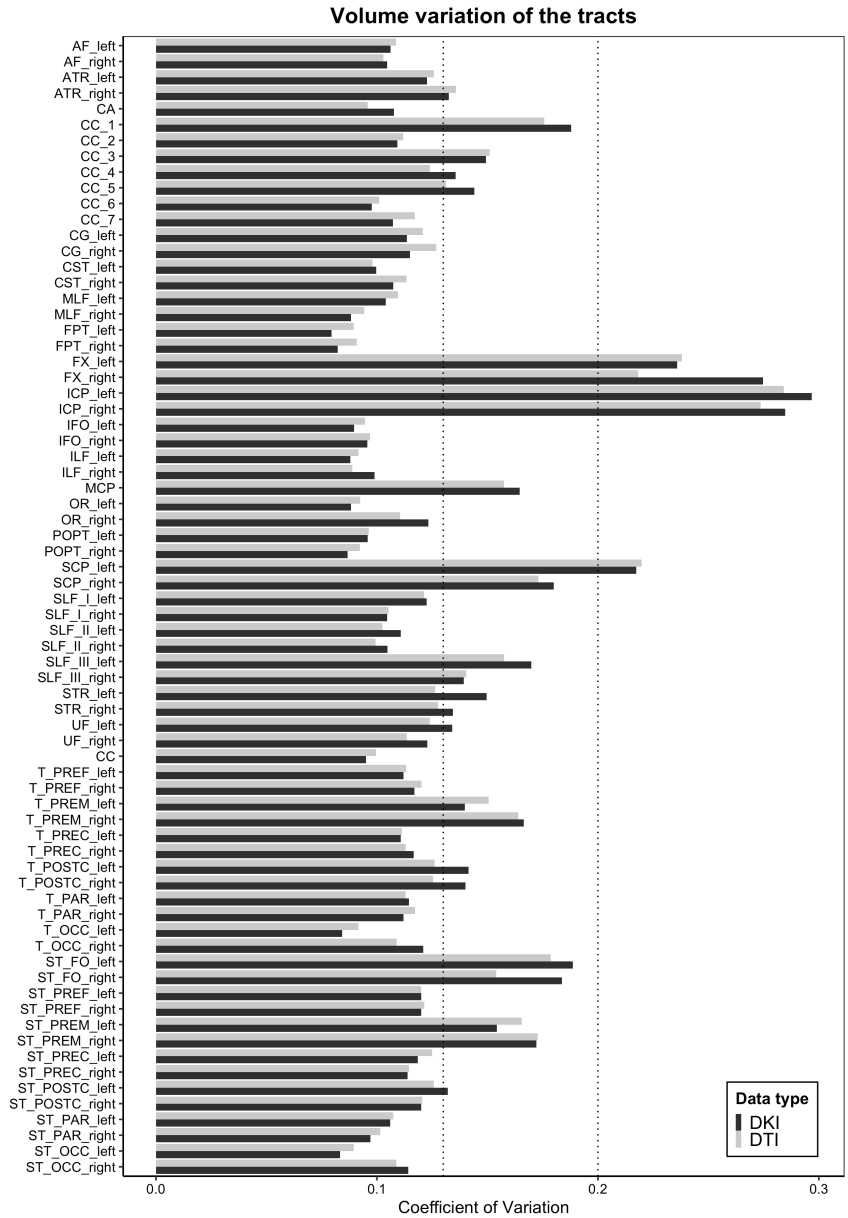

Figure 5.3: Coefficient of variation of the normalized volume for each tract. A list with all abbreviations for the studied nerve tracts can be found in Appendix A.1

5.2 Data Analysis

5.2.1 Control of Normal Distribution

After controlling normal distribution with the Shapiro-Wilk test, the majority of the samples from the DTI data were normally distributed. Only 4.2% of the samples based on the FA parameter and 13.6% of the samples based on the MD parameter were found not to be normally distributed. Similar numbers were found on the DKI data, where 15.9% of the samples based on the FA parameter and 3.0% of the samples based on the MD parameter were not normally distributed. After the individual with a distorted DKI image was removed, 53% of the samples from the MK parameter were still not normally distributed.

5.2.2 Group Comparison

Welch's t-test

The use of Welch's t-test for each nerve tract compared the microstructure of the brain between the different groups. 66 nerve tracts were analyzed and hence, 66 different hypothesis tests were done for each of the five parameters and for the two different group-comparisons. The number of significant p-values of all these comparisons are summarized in Table 5.1. Significant differences were only found in two tracts in the comparison between the NPSLE and non-NPSLE. In the comparison between healthy controls and all SLE patients, significant differences were found in many tracts. The FA parameter, based on both the DKI and the DTI data, showed differences in the largest number of tracts. MD based on the DTI data also found differences in some of the tracts. All p-values for the the comparison between healthy controls and all SLE patients can be seen in Appendix A.2. When the significance level was corrected by Bonferroni correction to account for the multiple comparisons issue, only three tracts were found to be significantly different, as can be seen in Table 5.1.

The mean values for each group, based on FA, MD and MK can be seen in Figure 5.4, 5.5, and 5.6. Lower FA-values and higher MD-values are observed in all tracts for the SLE patients than for the healthy controls. However, the difference is only significant in a number of the tracts, based in the information in Table 5.1. The mean values for the MK parameter in each tract do not have the same order of the different groups.

The difference between the two classifications of SLE does not show large significance based on the method used in this thesis. Studying Figure 5.4, a lower mean FA in each tract for the NPSLE group than the non-NPSLE group can be

observed. The difference is not significant, but the trend can be seen in almost every studied tract.

Table 5.1: A summation of all hypothesis tests and how many significant differences were found. The first number is the number of significant differences found without correction for multiple comparisons, and within parenthesis is the number of significant differences after the correction.

	Number of tracts with significant differences	
Data set, parameter	**HC - SLE**	**NPSLE - non-NPSLE**
DTI, FA	54 (3)	1 (0)
DTI, MD	19 (0)	0 (0)
DKI, FA	38 (0)	1 (0)
DKI, MD	0 (0)	0 (0)
DKI, MK	0 (0)	0 (0)

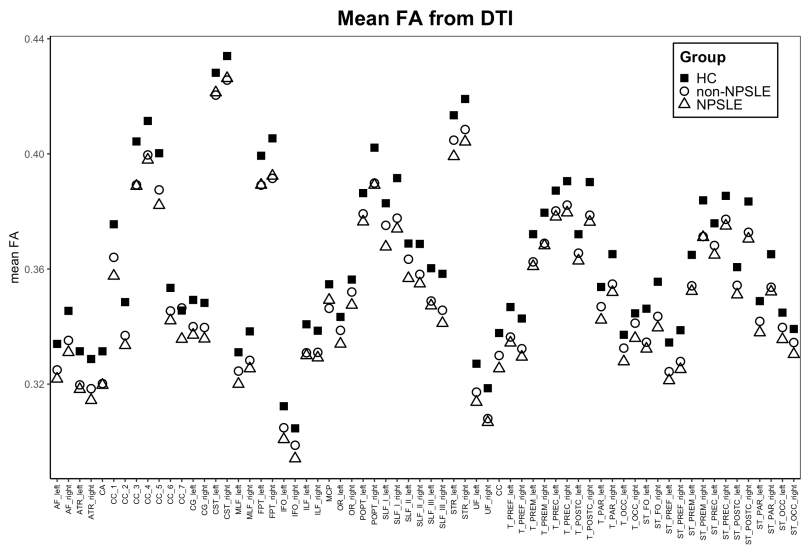

Figure 5.4: Mean values of FA for the three groups in each tract. Note that the values are in the same order for the majority of the tracts, healthy controls having the largest value and NPSLE having the lowest value.

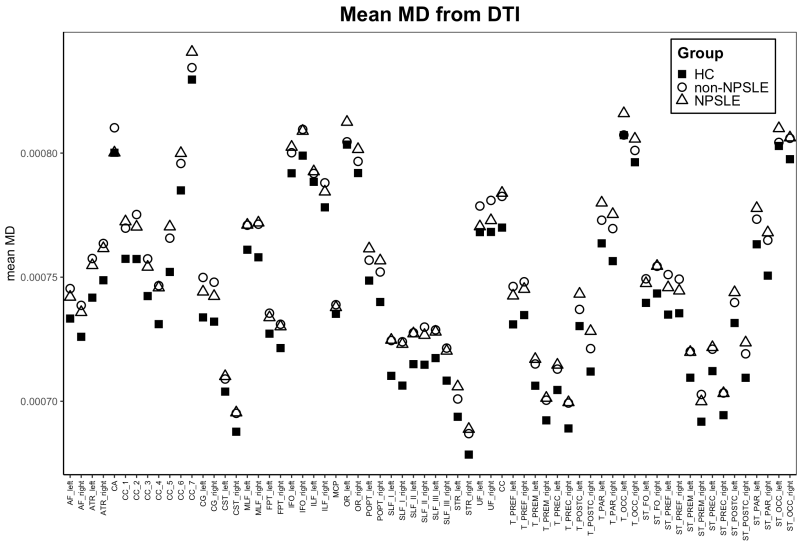

Figure 5.5: Mean values of MD for the three groups in each tract. Note that mean value for the healthy control group is the lowest value in every tract.

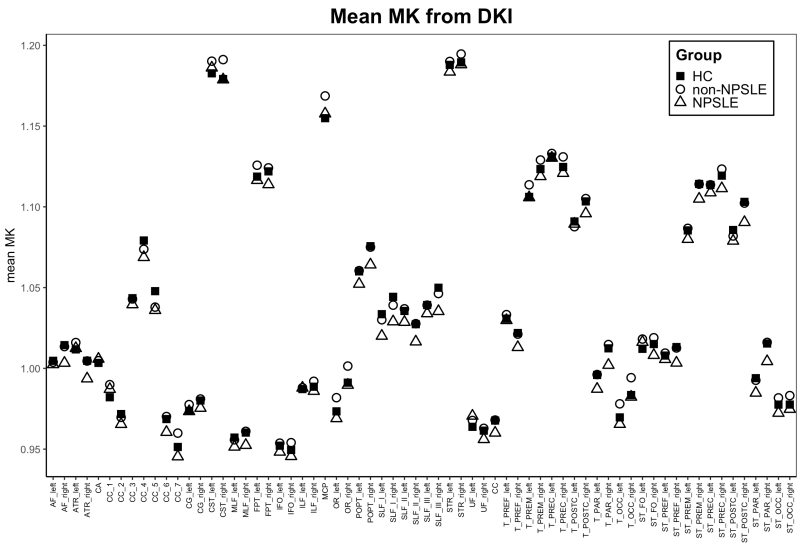

Figure 5.6: Mean values of MK for the three groups in each tract.

Principal Component Analysis

The principal component analysis included information from all studied tracts and made group-comparison based on this. Dimensionality reduction for each individual from 66 dimensions, with all studied nerve tracts, to only one dimension still included over 70 % of the variance for all five parameters, see Table 5.2. Doing a Welch's t-test on the first principal component showed significance between the healthy controls and all SLE patients when using the FA values based on the DTI and the DKI data. No significant differences were found based on the first principal component between NPSLE and non-NPSLE. A summary of all p-values can be seen in Table 5.2. In Figure 5.7, principal component 1 and 2 are plotted for the FA values from the DTI data. It can be seen that there is a larger spread of the SLE patients than for the healthy controls.

Table 5.2: Summary of p-values for the first principal component for each parameter.

Parameter	p, HC - SLE	p, NPSLE - non-NPSLE	PC1, Variance
FA, DTI	**0.002**	0.44	74.4%
MD, DTI	0.06	0.96	78.3%
FA, DKI	**0.02**	0.43	77.1%
MD, DKI	0.36	0.67	80.4%
MK, DKI	0.80	0.59	86.2%

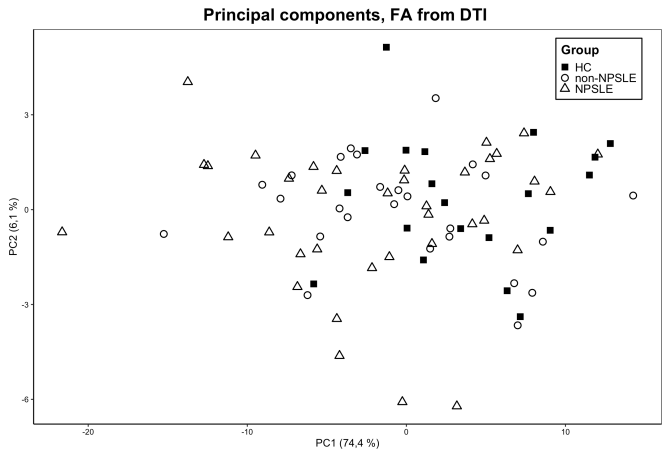

Figure 5.7: Plot with the two first principal components of mean FA values based on the DTI data.

5.2.3 Effect Size

Investigation of the effect size was done to find the method giving the highest statistical power in the group comparison. The effect size of the differences between the two classifications of SLE were small, with $d < 0.5$, in all tracts. Due to the low effect size it is not possible to draw any conclusions on the statistical power based on this comparison.

Larger effects were found in the comparison between HC and SLE. No significant differences and no effect sizes larger than 0.5 were found in the comparison based on MD and MK from the DKI data. The effect size for the other three parameters in the comparison between HC and SLE can be seen in Figure 5.9. In the majority of the tracts, the effect size is largest for the FA value from the DTI data.

Studying the effect size of different tracts can also tell where the differences between the groups are largest. The corticospinal tract and the optic radiation had low effect sizes and were not significant for any of the sides, left or right. The largest effect size was found in the left Anterior Thalamic Radiation, ATR_left in Figure 5.9, for the FA parameter based on the DTI data. The estimated normal distributions and the corresponding data points from this comparison can be seen in Figure 5.8. The mean values of the data points can be separated, and it can also be seen that the data points overlap each other from the two groups. The spread of the values for the SLE patients is wider than the spread for the healthy controls.

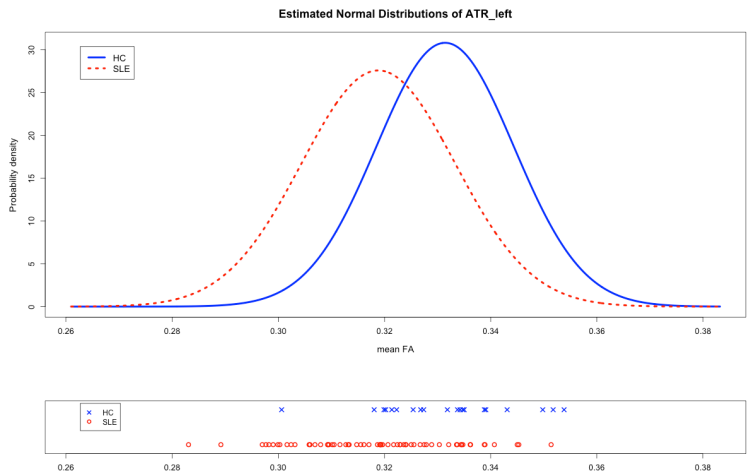

Figure 5.8: The estimated normal distributions and corresponding data points from the left Anterior Thalamic Radiation, ATR_left, that was found to have the largest effect size.

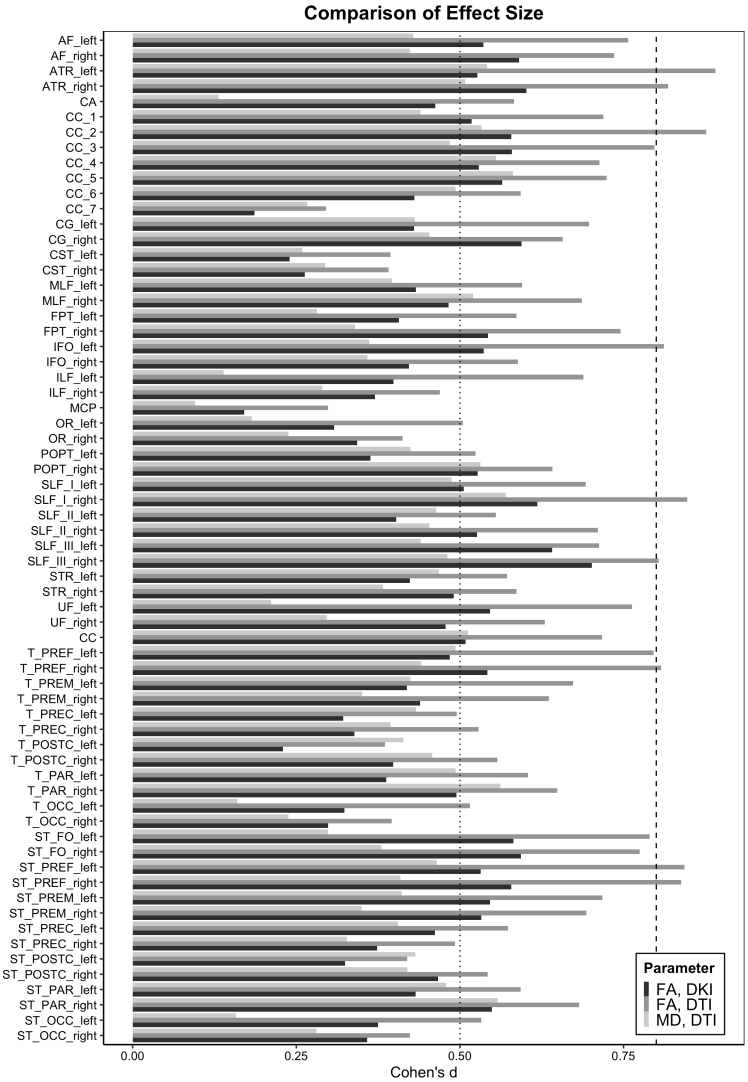

Figure 5.9: Comparison of Cohen's d on three of the studied parameters for each tract. The effect size is largest for the FA parameter from the DTI data in the majority of the tracts. The dotted and the dashed lines mark where the effect size is defined to be medium, $d = 0.5$, and large, $d = 0.8$.

Chapter 6
Discussion

6.1 Pipeline

The aim of this thesis was to find a way to enable group-comparisons of the whole brain by include all major nerve tracts of the brain. A methodology was identified and implemented that enables the analysis of the microstructure of the major nerve tracts, without requiring time-consuming manual work. The new approach to extract parameters of the white matter microstructure enabled group comparison between the SLE patients and healthy controls, although some nerve tracts had to be removed due to incomplete segmentation.

6.1.1 Importance of Quality Control

The use of automated methods, without any manual work, enables analysis of large data sets. The output from the pipeline is parameters representing the tract for each individual. In order to make sure that every step of the pipeline is properly done, it is of importance to have thorough quality control of each step.

The visual inspection of the quality control was found not to be sufficient. The image with the 2D projections of all tracts for each individual, see Figure 5.1, made it easier to visually inspect the segmentation than to check all 3D images. Without any prior knowledge about how the tracts should look like, it was hard to see if the segmentations were correct or not.

The use of the coefficient of variation of the volumes in each tract for all individuals was an attempt to quantify the segmentations. This type of quality control is still a relative measure. If the segmentation of one tract is wrong in all individuals, the coefficient of variation will not make this wrongly segmented tract to be found. To be able to make a proper quality control of the nerve tracts, a ground truth would be needed. How to find the ground truth for the segmentation is also

a problem. It could be possible to use an atlas of the segmentations in a standard brain and project this atlas into the individual space. This would lead to the possibility of comparing the result with the correct segmentation. The segmentation of nerve tracts based on the diffusion of the brain are estimations of the nerve tracts. Hence, the real ground truth of each individual is somehow unknown until the day the brain could be dissected. A nerve tract with deviant segmentation might occur due to pathology of the brain or due to mistakes of the segmentation method.

6.2 Statistical Power

In the development of a new methodology, it is important to consider the statistical power. Inducing variance in any of the steps to extract the values will lower the effect size and hence, lower the statistical. One important step in the analysis was to remove the tracts with the highest C_v, and thereby not induce any noise from the wrongly segmented tracts.

Based on the method and statistical analysis used in this thesis, it was found that the FA value based on the DTI data gave the largest effect size and would be preferred to find differences between the different groups. In previous studies where the statistical power between different parameters are compared, the MK parameter based on DKI have been shown to give the largest statistical power. In a study on brain maturation, the DKI was found to offer a more sensitive detection of tissue microstructural changes [28]. Another study of the microstructure of the development of the brain showed that larger between-group differences were found based on DKI than on DTI [29]. The result of the investigated effect size in this thesis is not in line with these previous studies where the microstructure is compared. In the statistical analysis of this work, no significant differences were found in the MK parameter.

The difference of the results between DKI and DTI might be due to the lower resolution of the DKI data. The extraction of the parameters based on the DKI data might also have been affected by the smoothing in the preprocessing step. The DTI data was not in the need of any smoothing. A major part of the group samples from the MK parameter were also found not to be normally distributed. Welch's t-test was still used for the comparison of these values. The time limitation of this project restricted me to look further into the DKI data and why it behaved differently than the DTI data. Before any conclusions could be drawn that the DTI analysis gives higher statistical power than the DKI analysis, the control of the analysis on the DKI needs further analysis.

6.3 Group Comparison

Previous results on the same data was confirmed, where significant differences of the microstructure of the brain was found when comparing HC and SLE. Lower FA values and higher MD values in the SLE patients are indications that there are microstructural damages of the white matter in these patients. In Figure 5.4, it could also be seen that the mean value of FA was slightly smaller for the NPSLE group than the non-NPSLE group in the majority of tracts. No significant differences were found by the statistical tests, but it might still be an indication that the NPSLE patients have a larger fraction of abnormalities of the white matter. These findings emphasize the theory that all SLE patients suffer from white matter abnormalities, not only the patients classified with NPSLE. It is also an indication that the classification into NPSLE and non-NPSLE is uncertain.

Another interesting finding in the comparison between healthy controls and SLE patients was the correlation of the nerve tracts where no significant was found with the function of the tract. The corticospinal tract and the optic radiation did not show any significant differences when comparing the FA values. These tracts are mainly involved in motor tasks or transferring of visual signals. SLE patients typically do not have problem with this, which is why it was not expected to be any differences between healthy controls and SLE patients in these areas.

When solving the multiple comparison problem by the use of Bonferroni correction, no significant differences was found. One could discuss if the results are reliable when the difference between the groups are said to be significant when no corrections was done for multiple comparisons. The comparison between the groups can be seen in two different ways: considering the whole brain or comparing tract by tract. Doing 66 hypothesis tests, one for each tract, and stating significant differences in the whole brain will not be valid without the correction for multiple comparisons. To do proper comparisons where the whole brain should be analyzed, the use of principal component analysis is a better approach. In case different parts of the brain should be compared, and with the aim is to find where there are differences between the group, the hypothesis test of each tract can be seen as independent. The significance level without the correction for multiple comparisons could still be valid in this case.

6.3.1 Comparing Methodology with the Previous Analysis

The methods for the segmentation differ between the work in this thesis and the previous analysis of the same data. This makes it hard to do a proper comparison of the results. The segmentation in the previous work only cover the most central part

of each tract. In this thesis, the segmentation of the nerve tracts includes a larger fraction, and the more peripheral parts, of each tract. The fact that a larger part of the tract is included might be beneficial if the alterations of the white matter is widely spread in the tracts. If the alterations of the white matter occur in the center of each, the inclusion of a larger volume for each tract will only introduce more noise and hence, the statistical power will be decreased. Significant differences were found in some of the tracts, where the previous analysis showed that the difference was not significant. This is an indication that the segmentation method in this thesis is more sensitive in the way of finding differences between the groups of individuals.

6.4 Future Work

The mean value of each calculated parameter was used as the representation for every tract. It is a common way of representing each tract with one value, and that was why it was chosen. Investigating other ways of doing the representation of each tract would be interesting. One question that needs to be answered is: are the parameter values within each tract normally distributed? In case of a skewed distribution, another way of extracting the value would lead to a better representation of that tract. Future work could include investigating different ways to represent the tracts with one value and if it could lead to higher statistical power.

The time limitation of this thesis restricted the statistical analysis. The results from the statistical analysis can be seen as preliminary and future work will be required to extend the analysis. Previous analysis on the same data set included correlation of parameter values with the disease duration, cognitive tests, age, and results from the blood tests. With values for a larger number of tracts, this analysis could be extended and could lead to new insights about the disease.

6.5 Ethical Aspects

All individuals that was part of the study have given their informed consent in being a part of the study. The study also had ethical approval for being performed. One ethical aspect to consider in studies is the anonymity. The privacy of each individual should be protected. This is why the personal information, such as the personal identity number, of each individual is not saved in the data that other people have access to. When 3D images of the head are gathered, especially MRI where soft tissue can be imaged, it is possible to reconstruct the face of each individual. Facial information can be used to identify the individual and thereby

the anonymity is not protected. There are software that can be used to remove facial data and thereby achieve anonymity [30]. In this thesis, no 3D images of the head of any individual is presented and thus, the anonymity is still kept but it is an important aspect to consider when 3D images are handled.

In group studies where healthy controls should be included, it is harder to motivate the inclusion of healthy controls in studies where the imaging technology is doing any harm for the individual. MRI has the large advantage of not involving any ionizing radiation. It is not harmful for individuals and hence, including healthy individuals in studies based on MRI is not an ethical problem. Even though it is not harmful, some individuals might experience the acquisition to be uncomfortable. The tunnel of the scanner is small, which can lead to a claustrophobic feeling, and the high volume of the sound from the scanner might seem intimidating.

Chapter 7
Conclusion

The use of a method where the segmentation of nerve tracts does not require time-consuming manual work enables the analysis to cover a larger part of the brain. When several steps of a methodology are implemented in a pipeline, extensive quality control is required to ensure the quality of each step.

The results from the group comparison are in line with previous research of SLE. Significant difference were found in several tracts when comparing the healthy controls with the SLE patients with the FA value being lowered for the SLE patients. Lower FA values indicates damage of the white matter in SLE patients. Almost no significant differences were found when comparing the subgroups of SLE, NPSLE and non-NPSLE. This further emphasizes the theory of the brain being affected in all SLE patients, and not only the ones having neuropsychiatric symptoms.

Based on the statistical analysis done, the FA parameter from the DTI data was found to give the highest statistical power of the group comparison. The MK parameter from the DKI did not show any differences between the groups. This is not in line with previous studies and must be investigated further in the methodology of the pipeline.

Chapter A
Appendix

A.1 Abbreviations of all Nerve Tracts

Table A.1: Abbreviations of the names of the nerve tracts.

Abbreviation	Name of the Nerve Tract
AF_left	Arcuate fascicle
AF_right	
ATR_left	Anterior Thalamic Radiation
ATR_right	
CA	Commissure Anterior
CC_1	Rostrum
CC_2	Genu
CC_3	Rostral body (Premotor)
CC_4	Anterior midbody (Primary Motor)
CC_5	Posterior midbody (Primary Somatosensory)
CC_6	Isthmus
CC_7	Splenium
CG_left	Cingulum
CG_right	
CST_left	Corticospinal tract
CST_right	
MLF_left	Middle longitudinal fascicle
MLF_right	
FPT_left	Fronto-pontine tract
FPT_right	
FX_left	Fornix
FX_right	

Table A.1 continued from previous page

Abbreviation	Name of the Nerve Tract
ICP_left	Inferior cerebellar peduncle
ICP_right	
IFO_left	Inferior occipito-frontal fascicle
IFO_right	
ILF_left	Inferior longitudinal fascicle
ILF_right	
MCP	Middle cerebellar peduncle
OR_left	Optic radiation
OR_right	
POPT_left	Parieto-occipital pontine
POPT_right	
SCP_left	Superior cerebellar peduncle
SCP_right	
SLF_I_left	Superior longitudinal fascicle I
SLF_I_right	
SLF_II_left	Superior longitudinal fascicle II
SLF_II_right	
SLF_III_left	Superior longitudinal fascicle III
SLF_III_right	
STR_left	Superior Thalamic Radiation
STR_right	
UF_left	Uncinate fascicle
UF_right	
CC	Corpus Callosum - all
T_PREF_left	Thalamo-prefrontal
T_PREF_right	
T_PREM_left	Thalamo-premotor
T_PREM_right	
T_PREC_left	Thalamo-precentral
T_PREC_right	
T_POSTC_left	Thalamo-postcentral
T_POSTC_right	
T_PAR_left	Thalamo-parietal
T_PAR_right	
T_OCC_left	Thalamo-occipital
T_OCC_right	
ST_FO_left	Striato-fronto-orbital

Table A.1 continued from previous page

Abbreviation	Name of the Nerve Tract
ST_FO_right	
ST_PREF_left	Striato-prefrontal
ST_PREF_right	
ST_PREM_left	Striato-premotor
ST_PREM_right	
ST_PREC_left	Striato-precentral
ST_PREC_right	
ST_POSTC_left	Striato-postcentral
ST_POSTC_right	
ST_PAR_left	Striato-parietal
ST_PAR_right	
ST_OCC_left	Striato-occipital
ST_OCC_right	

A.2 Group Comparison

Table A.2: p-values of the comparison between healthy controls and patients with SLE with Welch's t-test. Bold number shows a significance, with p-value smaller than 0.05 and the asterisk marks the number where the comparison is significant after correcting for multiple comparisons.

	$p_{DTI, FA}$	$p_{DTI, MD}$	$p_{DKI, FA}$	$p_{DKI, MD}$	$p_{DKI, MK}$
AF_left	**0.003**	0.088	**0.018**	0.395	0.864
AF_right	**0.001**	0.083	**0.006**	0.181	0.504
ATR_left	**0.001**	**0.041**	**0.018**	0.478	0.845
ATR_right	**0.001**	**0.045**	**0.010**	0.130	0.558
CA	**0.024**	0.594	**0.046**	0.774	0.884
CC_1	**0.002**	0.075	**0.017**	0.971	0.645
CC_2	**0.0003***	**0.041**	**0.008**	0.280	0.676
CC_3	**0.001**	**0.070**	**0.008**	0.679	0.833
CC_4	**0.005**	**0.025**	**0.027**	0.386	0.422
CC_5	**0.002**	**0.007**	**0.022**	0.214	0.325
CC_6	**0.007**	**0.018**	0.060	0.197	0.625
CC_7	0.300	0.215	0.502	0.712	0.988
CG_left	**0.003**	0.086	**0.049**	0.596	0.897
CG_right	**0.005**	0.074	**0.012**	0.391	0.841
CST_left	0.096	0.280	0.320	0.955	0.686
CST_right	0.113	0.220	0.283	0.978	0.707
MLF_left	**0.013**	0.089	0.061	0.203	0.640
MLF_right	**0.002**	**0.024**	**0.022**	0.194	0.626
FPT_left	**0.011**	0.259	0.068	0.726	0.883
FPT_right	**0.002**	0.165	**0.025**	0.435	0.742
IFO_left	**0.002**	0.125	**0.019**	0.279	0.842
IFO_right	**0.008**	0.091	0.066	0.396	0.960
ILF_left	**0.013**	0.565	0.101	0.712	0.932
ILF_right	0.071	0.216	0.137	0.545	0.985
MCP	0.209	0.630	0.517	0.840	0.570
OR_left	0.067	0.422	0.240	0.753	0.904
OR_right	0.105	0.269	0.205	0.810	0.718
POPT_left	**0.022**	0.052	0.116	0.182	0.621
POPT_right	**0.004**	**0.010**	**0.020**	0.071	0.454
SLF_I_left	**0.008**	**0.049**	**0.028**	0.257	0.403
SLF_I_right	**0.0003***	**0.016**	**0.006**	0.140	0.305
SLF_II_left	**0.017**	0.059	**0.046**	0.403	0.730

Table A.2 continued from previous page

	$p_{DTI, FA}$	$p_{DTI, MD}$	$p_{DKI, FA}$	$p_{DKI, MD}$	$p_{DKI, MK}$
SLF_II_right	**0.002**	0.060	**0.013**	0.301	0.561
SLF_III_left	**0.002**	0.085	**0.006**	0.437	0.776
SLF_III_right	**0.0003***	**0.042**	**0.002**	0.159	0.360
STR_left	**0.024**	**0.046**	0.100	0.663	0.903
STR_right	**0.018**	0.105	0.054	0.870	0.919
UF_left	**0.005**	0.423	**0.012**	0.947	0.632
UF_right	**0.013**	0.251	**0.046**	0.453	0.810
CC	**0.003**	**0.024**	**0.030**	0.188	0.616
T_PREF_left	**0.002**	0.064	**0.027**	0.459	0.969
T_PREF_right	**0.001**	0.077	**0.022**	0.261	0.629
T_PREM_left	**0.004**	0.086	0.057	0.865	0.807
T_PREM_right	**0.012**	0.134	0.062	0.729	0.983
T_PREC_left	**0.045**	0.090	0.178	0.687	0.977
T_PREC_right	**0.028**	0.088	0.151	0.699	0.972
T_POSTC_left	0.110	0.052	0.318	0.409	0.853
T_POSTC_right	**0.021**	**0.024**	0.100	0.220	0.778
T_PAR_left	**0.008**	**0.020**	0.084	0.130	0.547
T_PAR_right	**0.003**	**0.006**	**0.025**	0.107	0.580
T_OCC_left	0.062	0.485	0.213	0.764	0.893
T_OCC_right	0.120	0.274	0.258	0.878	0.684
ST_FO_left	**0.002**	0.275	**0.010**	0.872	0.698
ST_FO_right	**0.002**	0.141	**0.011**	0.508	0.850
ST_PREF_left	**0.001**	0.090	**0.015**	0.399	0.951
ST_PREF_right	**0.001**	0.111	**0.013**	0.259	0.591
ST_PREM_left	**0.002**	0.137	**0.017**	0.496	0.818
ST_PREM_right	**0.006**	0.153	**0.020**	0.506	0.683
ST_PREC_left	**0.013**	0.124	**0.048**	0.466	0.800
ST_PREC_right	**0.030**	0.144	0.103	0.546	0.796
ST_POSTC_left	0.070	0.057	0.157	0.236	0.624
ST_POSTC_right	**0.018**	**0.038**	**0.049**	0.127	0.512
ST_PAR_left	**0.007**	**0.028**	**0.049**	0.112	0.472
ST_PAR_right	**0.002**	**0.007**	**0.013**	0.086	0.480
ST_OCC_left	**0.038**	0.492	0.116	0.577	0.866
ST_OCC_right	0.067	0.197	0.159	0.685	0.935

References

[1] A. A. Bengtsson and L. Rönnblom, "Systemic lupus erythematosus: still a challenge for physicians," *Journal of internal medicine*, vol. 281, pp. 52–64, 2017.

[2] A. Baird and S. Warach, "Magnetic resonance imaging of acute stroke," *Journal of Cerebral Blood Flow & Metabolism*, vol. 18, no. 6, pp. 583–609, 1998.

[3] H. Larsson, C. Thomsen, J. Frederiksen, M. Stubgaard, and O. Henriksen, "In vivo magnetic resonance diffusion measurement in the brain of patient with multiple sclerosis," *Magnetic Resonance Imaging*, vol. 10, no. 1, pp. 7–12, 1992.

[4] K. Kono, Y. Inoue, K. Nakayama, M. Shakudo, M. Morino, K. Ohata, K. Wakasa, and R. Yamada, "The role of diffusion-weighted imaging in patients with brain tumors," *American Journal of Neuroradiology*, vol. 22, no. 6, pp. 1081–1088, 2001.

[5] J. Nystedt, M. Nilsson, A. Jönsen, P. Nilsson, A. Bengtsson, A. Lilja, J. Lätt, P. Mannfolk, and P. C. Sundgren, "Altered white matter microstructure in lupus patients: a diffusion tensor imaging study," *Arthrisis Research & Therapy*, 2018.

[6] L. Klareskog, T. Saxne, A. Rudin, L. Rönnblom, and Y. Enman, *Reumatologi*. Studentlitteratur, 3 ed., 2017. pp. 177-188.

[7] R. Cervera, M. Khamashta, and H. GR, "The euro-lupus project: epidemiology of systemic lupus erythematosus in europe," *Lupus*, vol. 18, pp. 869–874, 2009.

[8] "The american college of rheumatology nomenclature and case definitions for neuropsychiatric lupus syndromes," *Arthrisis & Rheumatism*, vol. 42, no. 2, pp. 599–608, 1999.

[9] J. G. Betts, K. A. Young, J. A. Wise, E. Johnson, B. Poe, D. H. Kruse, O. Korol, J. E. Johnson, M. Womble, and P. DeSaix, *Anatomy and Physiology*. OpenStax, 2017. pp. 505-506, 512.

[10] E. Stejskal and J. E. Tanner, "Spin diffusion measurements: spin echoes in the presence of time-dependent field gradient," *The Journal of Chemical Physics*, vol. 42, no. 1, pp. 288–292, 1965.

[11] P. J. Basser, J. Mattiello, and D. LeBihan, "Mr diffusion tensor spectroscopy and imaging," *Biophysical Journal*, vol. 66, pp. 259–267, 1994.

[12] J. H. Jensen, J. A. Helpern, A. Ramani, H. Lu, and K. Kaczynski, "Diffusional kurtosis imaging: The quantification of non-gaussian water diffusion by means of magnetic resonance imaging," *Magnetic Resonance in Medicine*, vol. 53, pp. 1432–1440, 2005.

[13] A. Arab, A. Wojna-Pelczar, A. Khaimar, N. Szabó, and J. Ruda-Kucerova, "Principles of diffusion kurtosis imaging and its role in early diagnosis in neurodegenerative disorders," *Brain Research Bulletin*, vol. 139, pp. 91–98, 2018.

[14] J. H. Jensen and J. A. Helpern, "Mri quantification of non-gaussian water diffusion by kurtosis analysis," *NMR in Biomedicine*, vol. 23, pp. 698–710, 2010.

[15] F. Dell'Acqua and J. D. Tournier, "Modelling white matter with spherical deconvolotuon: How and why?," *NMR in Biomedicine*, vol. 32, no. 4, p. e3945, 2019.

[16] J.-D. Tournier, F. Calamante, D. G. Gadian, and A. Connelly, "Direct estimation of the fiber orientation density function from diffusion-weighted mri data using spherical deconvolution," *NeuroImage*, vol. 23, pp. 1176–1185, 2004.

[17] J.-D. Tournier, F. Calamante, and A. Connelly, "Robust determination of the fibre orientation distribution in diffusion mri: Non-negativity constrained super-resolved spherical deconvolution," *NeuroImage*, vol. 35, pp. 1459–1472, 2007.

[18] F.-C. Yeh, "High-definition fiber tracking created using dsi studio (http://dsi-studio.labsolver.org)." CC BY-SA (https://creativecommons.org/licenses/by-sa/4.0), 2019.

[19] I. Aganj, "Automatic verification of the gradient table in diffusion-weighted mri based on fiber continuity," *Scientific Reports*, vol. 8, no. 16541, 2018.

[20] J. Wasserthal, P. Neher, and K. H. Maier-Hein, "Tractseg - fast and accurate white matter tract segmentation," *NeuroImage*, vol. 183, pp. 239 – 253, Aug. 2018.

[21] P.-L. Bazin, C. Ye, J. A. Bogovic, N. Shiee, D. S. Reich, J. L. Prince, and D. L. Pham, "Direct segmentation of the major white matter tracts in diffusion tensor images," *NeuroImage*, vol. 58, no. 2, pp. 458 – 468, 2011.

[22] J. Cohen, *Statistical Power Analysis for the Behavioral Sciences*. Hillsdale : L. Erlbaum Associates, 2. ed. ed., 1988. pp. 25-26, 66-67.

[23] K. Gorgolewski, C. D. Burns, C. Madison, D. Clark, Y. O. Halchenko, M. L. Waskom, and S. S. Ghosh, "Nipype: a flexible, lightweight and extensible neuroimaging data processing framework in python," *Frontiers in Neuroinformatics*, vol. 5, Aug. 2011.

[24] J.-D. Tournier, R. Smith, D. Raffelt, R. Tabbara, T. Dhollander, M. Pietsch, D. Christiaens, B. Jeurissen, C.-H. Yeh, and A. Connelly, "Mrtrix3: A fast, flexible and open software framework for medical image processing and visualisation," *NeuroImage*, vol. 202, no. 116137, 2019.

[25] S. M. Smith, M. Jenkinson, M. W. Woolrich, C. F. Beckmann, T. E. Behrens, H. Johansen-Berg, P. R. Bannister, M. D. Luca], I. Drobnjak, D. E. Flitney, R. K. Niazy, J. Saunders, J. Vickers, Y. Zhang, N. D. Stefano], J. M. Brady, and P. M. Matthews, "Advances in functional and structural mr image analysis and implementation as fsl," *NeuroImage*, vol. 23, pp. 208 – 219, 2004.

[26] E. Garyfallidis, M. Brett, B. Amirbekian, A. Rokem, S. van der Walt, M. Descoteaux, I. Nimmo-Smith, and Dipy Contributors, "Dipy, a library for the analysis of diffusion mri data," *Frontiers in Neuroinformatics*, vol. 8, 2014.

[27] RStudio Team, *RStudio: Integrated Development Environment for R*. RStudio, Inc., Boston, MA, 2016.

[28] M. M. Cheung, E. S. Hui, K. C. Chan, J. A. Helpern, L. Qi, and E. X. Wu, "Does diffusion kurtosis imaging lead to better neural tissue characterization? a rodent brain maturation study," *NeuroImage*, vol. 45, p. 386—392, April 2009.

[29] F. Grinberg, I. Maximov, E. Farrher, I. Neuner, L. Amort, H. Thoennessen, E. Oberwelland, K. Konrad, and N. Shah, "Diffusion kurtosis metrics as biomarkers of microstructural development: A comparative study of a group of children and a group of adults," *NeuroImage*, vol. 144, 09 2016.

[30] A. Bischoff-Grete, I. Burak Ozyurt, E. Busa, B. T. Quinn, C. Fennema-Notestine, C. C. P., S. Morris, M. W. Bondi, T. L. Jernigan, A. M. Dale, G. G. Brown, and B. Fischl, "A technique for the deidentification of structural brain mr images," *Human Brain Mapping*, vol. 28, pp. 892–903, 2007.